Published in Chemistry - A European Journal 17, issue 35, 9669-9667, 2011
which should be used for any reference to this work

Excellent Correlation between Drug Release and Portal Size in Metalla-Cage Drug-Delivery Systems

Nicolas P. E. Barry,[a] Olivier Zava,[b] Paul J. Dyson,*[b] and Bruno Therrien*[a]

[a] N. P. E. Barry, Dr. B. Therrien
Institute of Chemistry, University of Neuchatel Ave de Bellevaux 51, 2000 Neuchatel (Switzerland) Fax: (+41) 32-718-2511
E-mail: bruno.therrien@unine.ch

[b] Dr. O. Zava, Prof. Dr. P. J. Dyson
Institut des Sciences et Ingénierie Chimique Ecole Polytechnique Fédérale de Lausanne (EPFL) CH-1015 Lausanne (Switzerland)
E-mail: paul.dyson@epfl.ch

Abstract: A series of large cationic hexanuclear metalla-prisms, $[Ru_6(p\text{-}iPrC_6H_4Me)_6(tpt)_2(donq)_3]^{6+}$, $[Ru_6(p\text{-}iPrC_6H_4Me)_6(tpt)_2(doaq)_3]^{6+}$ and $[Ru_6(p\text{-}iPrC_6H_4Me)_6(tpt)_2(dotq)_3]^{6+}$, composed of *p*-cymene–ruthenium building blocks bridged by *OO*∩*OO* ligands (donq = 5,8-dioxido-1,4-naphthoquinonato; doaq = 5,8-dioxido-1,4-anthraquinonato, dotq = 6,11-dioxido-5,12-naphthacenedionato) and connected by two 2,4,6-tripyridin-4-yl-1,3,5-triazine (tpt) panels, which encapsulate the guest molecules 1-(4,6-dichloro-1,3,5-triazin-2-yl)pyrene and $Pd(acac)_2$, have been prepared. The host–guest properties of these water-soluble delivery systems were studied in solution by NMR and fluorescence spectroscopy, providing the stability constants (*K*) for these host–guest systems. Moreover, the ability of the hosts to deliver the guests into cancer cells was evaluated and the uptake mechanism studied; the rate of release of the guest molecule was found to depend on the portal size of the host.

Keywords: bioorganometallic chemistry · drug delivery · endocytosis · host–guest systems · ruthenium

Introduction

In recent years the use of host–guest systems to efficiently deliver drugs to cancer cells has attracted much interest.[1] In such systems the physicochemical properties of the host–guest complex are generally superior to those of the guest alone leading to improvements in efficacy and biocompatibility.[2] It is not surprising that cisplatin,[3] the most widely used metal-based drug in the treatment of cancer, has been encapsulated in various hosts to reduce the severe side-effects associated with this drug.[4] Indeed, platinum-based drugs have been attached to various structures including carbon nanotubes,[5] proteins,[6] macrocycles[7] and dendrimers.[8] These large systems tend to accumulate preferentially in tumours due to enhanced permeability and retention (the EPR effect) of macromolecules in cancerous tissue.[9]

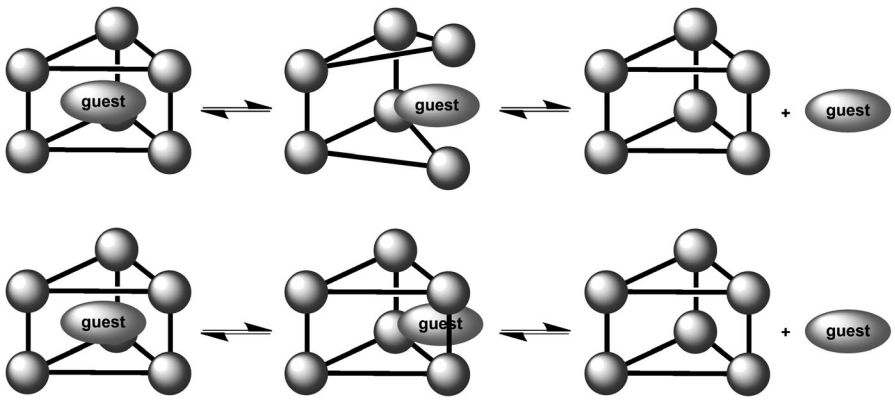

Figure 1. Guest-exchange mechanisms involving host rupture (top) or passage through an aperture (bottom).

The synthesis of discrete metalla-cages is now a well-established field in chemistry. Initially dominated by square-planar metal centres,[10] almost all transition metals have now been used in the preparation of metalla-cages.[11] The field is now entering a new era in which applications as sensors, micro-reactors or transporters are leading to new perspectives for metalla-cages.[12] These applications exploit the ability of metalla-cages to encapsulate and release guest molecules. This dynamic process involves different mechanisms depending on the nature of the metalla-cages, namely by partial rupture of the cage or by passage through an aperture.[13] These two reversible guest-exchange mechanisms are illustrated in Figure 1.

Recently we combined the medicinal properties of arene–ruthenium complexes, a promising class of organometallic drugs,[14] with aspects of supramolecular chemistry[15] to generate a new hybrid drug-delivery system, $[Ru_6(p\text{-}iPrC_6H_4Me)_6(tpt)_2(dobq)_3]^6$ (tpt = 2,4,6-tripyridin-4-yl)-1,3,5-triazine; dobq = 2,5-dioxido-1,4-benzoquinonato), in

which guest molecules were encapsulated into the cavity of the host. This host was found to encapsulate planar aromatic compounds[16] as well as planar platinum and palladium acetylacetonate (acac) complexes.[17] The biological activity of these compounds was evaluated on human ovarian cancer cell lines and the empty cage $[Ru_6(p\text{-}i\text{PrC}_6H_4Me)_6(tpt)_2(dobq)_3]^{6+}$ was found to have an IC_{50} value of 23 μM with the carceplexes being at least an order of magnitude more cytotoxic (the guests were not cytotoxic on their own).[17] The ability of this host to deliver guest molecules to cells was further confirmed by the encapsulation of a fluorescent-labelled pyrene-R derivative, 1-(4,6-dichloro-1,3,5-triazin-2-yl)pyrene.[18] Fluorescence experiments used to monitor the uptake of pyrene-R into cancer cells demonstrated an uptake of the carceplex $[\text{pyrene-R}\subset Ru_6(p\text{-}i\text{PrC}_6H_4Me)_6(tpt)_2(dobq)_3]^{6+}$ one order of magnitude greater than that of pyrene-R alone.[18] These systems suggest that after internalisation, the cage is destroyed in the cytoplasm and the release of the encapsulated molecule increases the cytotoxicity, thus giving rise to an additive effect.

In an extension to this work we have prepared a series of larger cationic hexanuclear metalla-prisms, $[Ru_6(p\text{-}i\text{PrC}_6H_4Me)_6(tpt)_2(donq)_3]^{6+}$ ($[\mathbf{1}]^{6+}$), $[Ru_6(p\text{-}i\text{PrC}_6H_4Me)_6(tpt)_2(doaq)_3]^{6+}$ ($[\mathbf{2}]^{6+}$) and $[Ru_6(p\text{-}i\text{PrC}_6H_4Me)_6(tpt)_2(dotq)_3]^{6+}$ ($[\mathbf{3}]^{6+}$) (donq = 5,8-dioxido-1,4-naphthoquinonato; doaq = 5,8-dioxido-1,4-anthraquinonato, dotq = 6,11-dioxido-5,12-naphthacenedionato) with similar sized cavities but different sized portals (Figure 2). Two guest molecules, $Pd(acac)_2$ and pyrene-R, were encapsulated into the cavities of these metalla-prisms and, in contrast to our previous work, no rupture of the host was necessary to release the guest. The stability constants of the host–guest systems involving pyrene-R were studied in solution by NMR and fluorescence spectroscopy and the anti-proliferative activities of the empty cages and of the host–guest systems $[Pd(acac)_2\subset\mathbf{1}\text{–}\mathbf{3}]^{6+}$ and $[\text{pyrene-R}\subset\mathbf{1}\text{–}\mathbf{3}]^{6+}$ were evaluated on human ovarian cancer cell lines. The uptake and release of pyrene-R by the $[\text{pyrene-R}\subset\mathbf{1}\text{–}\mathbf{3}]^{6+}$ systems were determined and correlated to the portal size of the host molecule.

Results and Discussion

The syntheses of the empty arene–ruthenium metalla-prisms $[\mathbf{1}]^{6+}$, $[\mathbf{2}]^{6+}$ and $[\mathbf{3}]^{6+}$ have been already described.[19,20] The cavities of $[\mathbf{1}\text{–}\mathbf{3}]^{6+}$ are of an equivalent size, but the use of different *OO*∩*OO* connectors controls their portal size, thus modulating the dynamics of the host–guest systems. The encapsulation of $Pd(acac)_2$ and pyrene-R in these cages requires the addition of silver triflate to the corresponding dinuclear arene–ruthenium complexes $[Ru_2(p\text{-}i\text{PrC}_6H_4Me)_2(OO\cap OO)Cl_2]$ (*OO*∩*OO* = donq, doaq and dotq) in the presence of the trigonal tpt panels and the guest molecule, leading to the connection of these different building blocks around the guest to afford $[Pd(acac)_2\subset\mathbf{1}\text{–}\mathbf{3}]^{6+}$ and $[\text{pyrene-R}\subset\mathbf{1}\text{–}\mathbf{3}]^{6+}$ (Scheme 1). All the metalla-prisms were isolated as triflate salts and characterised by IR, UV and NMR spectroscopy and by elemental analysis.

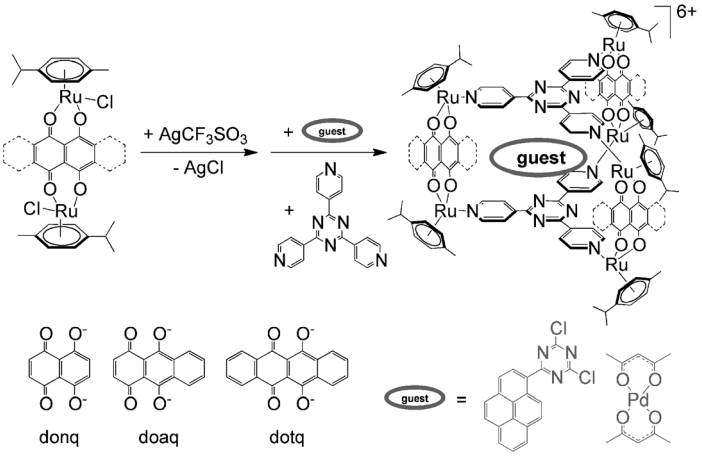

Scheme 1. Synthesis of $[\text{guest}\subset\mathbf{1}\text{–}\mathbf{3}]^{6+}$.

The formation of $[\text{guest}\subset\mathbf{1}\text{–}\mathbf{3}]^{6+}$ was monitored in CD_3CN by ^1H NMR spectroscopy. The resonances of the different protons of the guest molecule and the pyridyl protons of the tpt panels are shifted upfield upon formation of the encapsulated system, whereas the signals of the CH protons of the bridging ligands (donq, doaq or dotq) are shifted downfield. The proton resonances of the *p*-cymene ligands located at the periphery of the prism are not significantly affected by the presence of a guest molecule in the cavities of $[\mathbf{1}\text{–}\mathbf{3}]^{6+}$. In the ^1H NMR spectra of $[Pd(acac)_2\subset\mathbf{1}\text{–}\mathbf{3}]^{6+}$, the CH and CH_3 signals of the acetylacetato ligands are shifted upfield by around 1.7 ppm relative to the free complex, and in the spectra of $[\text{pyrene-R}\subset\mathbf{1}\text{–}\mathbf{3}]^{6+}$ the signals of the CH protons of the encapsulated aromatic guest are all shifted upfield relative to the free molecule, the frequencies being similar to those observed in $[\text{pyrene}\subset Ru_6(p\text{-}i\text{PrC}_6H_4Me)_6(tpt)_2(dobq)_3]^{6+}$.[16a]

The electronic absorption spectra of $[\text{guest}\subset\mathbf{1}\text{–}\mathbf{3}]^{6+}$ (see Figure 3) are characterised by an intense high-energy band centred at 300 nm, which may

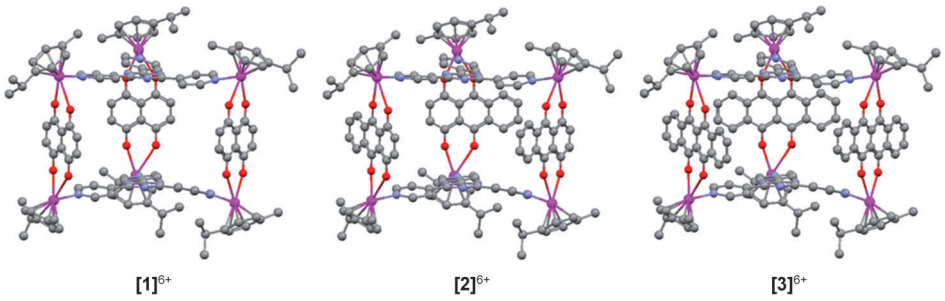

Figure 2. Molecular structures of the metalla-prisms $[\mathbf{1}]^{6+}$–$[\mathbf{3}]^{6+}$ (colour codes: magenta = Ru, red = O, purple = N, grey = C).

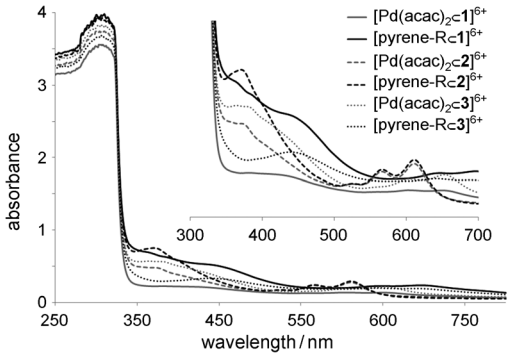

Figure 3. UV/Vis spectra of [guest⊂**1**–**3**]$^{6+}$ in CH_2Cl_2 (10^{-5} M).

be assigned to a ligand-localised or intra-ligand π→π* transition. In the visible region, a series of broad low-energy bands are observed and tentatively assigned to mixed metal-to-ligand charge-transfer (MLCT), intra-ligand charge-transfer (ILCT) and ligand π→π* transitions, with ILCT referring to intra-ligand charge transfer from the tpt panels to the *OO*∩*OO* bridging ligands.[21] In particular, in the electronic absorption spectra of [Pd(acac)$_2$⊂**2**]$^{6+}$ and [pyrene-R⊂**2**]$^{6+}$, two bands at 570 and 615 nm are remarkably well resolved, which is consistent with the spectrum of the empty metalla-prism [**2**]$^{6+}$.[20]

The infrared spectra of the metalla-prisms are dominated by absorptions of the coordinated *OO*∩*OO* bridging ligands. It is particularly noticeable that a significant redshift of about 20 cm^{-1} is observed for the C=O vibration frequencies of the quinone bridging ligands in all these spectra relative to the frequencies of the corresponding non-coordinated bridging ligands 5,8-dihydroxy-1,4-naphthoquinone, 5,8-dihydroxy-1,4-anthraquinone and 6,11-dihydroxy-5,12-naphthacenedione. This redshift can be attributed to a decrease in the CO bond order upon coordination to ruthenium atoms,[22] which is in accord with the X-ray data of the aquated metalla-clip [Ru$_2$(*p*-*i*PrC$_6$H$_4$Me)$_2$(donq)(OH$_2$)$_2$]$^{2+}$. Indeed, in this complex the lengths of the CO bonds are between 1.27(1) and 1.32(2) Å, which suggests an intermediate bond order between single (~1.40 Å) and double (~1.20 Å).[23] In addition to these C=O signals, strong absorptions due to the stretching vibrations of the triflate anions (1260 (s), 1030 (s), 638 cm^1 (m)) are observed in the infrared spectra of all the salts [Pd(acac)$_2$⊂**1**–**3**][CF_3SO_3]$_6$ and [pyrene-R⊂**1**–**3**][CF_3SO_3]$_6$.

The host–guest properties of the [guest⊂**1**–**3**]$^{6+}$ systems were studied in solution. We first established their stability in water, toluene and acetonitrile at room and elevated temperatures. The [Pd(acac)$_2$⊂**1**–**3**]$^{6+}$ systems show no signs of cage degradation or of leaching of the guest in any of the solvents tested, even after heating at reflux for 24 h, which is consistent with previous observations.[19] However, all [pyrene-R⊂**1**–**3**]$^{6+}$ systems show a rapid loss of the guest in [D$_8$]toluene at 80 °C but they remain intact in acetonitrile and water. The host–guest dynamics of the two systems [Pd(acac)$_2$⊂**1**–**3**]$^{6+}$ and [pyrene-R⊂**1**–**3**]$^{6+}$ are quite different. The most sterically demanding guest, Pd(acac)$_2$, is trapped in the cavities whereas the planar aromatic guest molecule, pyrene-R, leaches out of the cages. These observations suggest that the guest-release process involves a non-dissociative mechanism:[13] the apertures of the cages are large enough to allow pyrene-R to pass through, whereas Pd(acac)$_2$ is retained in the cavities of the cage compounds [**1**–**3**]$^{6+}$. To further study the encapsulation of pyrene-R in the metalla-prisms [**1**–**3**]$^{6+}$, diffusion-ordered NMR spectroscopy (DOSY) was performed.[24] As an example, the DOSY spectra of pyrene-R, [**1**]$^{6+}$ and pyrene-R + [**1**]$^{6+}$ in CD_3CN at room temperature are presented in Figure 4. These spectra show that at room temperature, [**1**]$^{6+}$ and pyrene-R + [**1**]$^{6+}$ possess almost identical diffusion coefficients, which confirms the encapsulation of pyrene-R in the hydrophobic cavity of [**1**]$^{6+}$. Similar results were obtained with metalla-prisms [**2**]$^{6+}$ and [**3**]$^{6+}$.

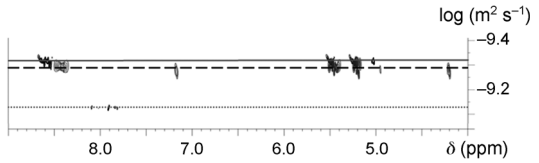

Figure 4. DOSY NMR spectra of pyrene-R (···), [**1**]$^{6+}$ (—) and [**1**]$^{6+}$ + 1 equivalent of pyrene-R (——) in CD_3CN at 21 °C.

We also confirmed the stoichiometry of the host–guest systems [pyrene-R⊂**1**–**3**]$^{6+}$ in CD_3CN and $(CD_3)_2SO$ by ^{1}H NMR titrations using the molar ratio method.[25] Upon gradual addition of pyrene-R (0.1–3.0 equiv) to a solution of the host (4.0 mM in CD_3CN and 10.0 mM in $(CD_3)_2SO$), changes in the chemical shifts of some protons were observed. The ^{1}H NMR spectra obtained from the titration experiments with [**3**]$^{6+}$ at 21 °C in CD_3CN are shown in Figure 5. The broadening and chemical shifts of the signals are indicative of a rapid inclusion of pyrene-R into the hydrophobic cavity of [**3**]$^{6+}$. Similar behaviour was observed in $(CD_3)_2SO$ although broadening of the pyridyl signals is

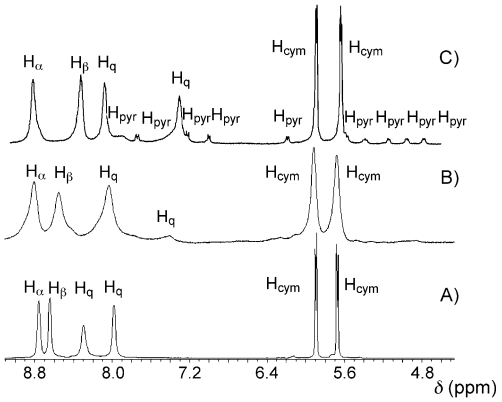

Figure 5. ^{1}H NMR titrations of pyrene-R in a solution of [**3**][CF_3SO_3]$_6$ in CD_3CN at 21 °C. A) [**3**]$^{6+}$ (4.0 mM), B) [**3**]$^{6+}$ + 0.5 equivalents of pyrene-R and C) [**3**]$^{6+}$ + 1.0 equivalent of pyrene-R.

more significant and the changes in chemical shifts of the signals corresponding to the pyrenyl protons are less pronounced.

Plots of the changes in the chemical shifts ($\Delta\delta$) of the signal of the H_β protons of the tpt ligands (CD_3CN) or of the signal of the H_q protons of the *OO*∩*OO* ligands ($(CD_3)_2SO$) versus the molar ratio of pyrene-R to the prisms $[\mathbf{1}–\mathbf{3}]^{6+}$ indicate the formation of 1:1 stoichiometric host–guest systems (see Figure 6).

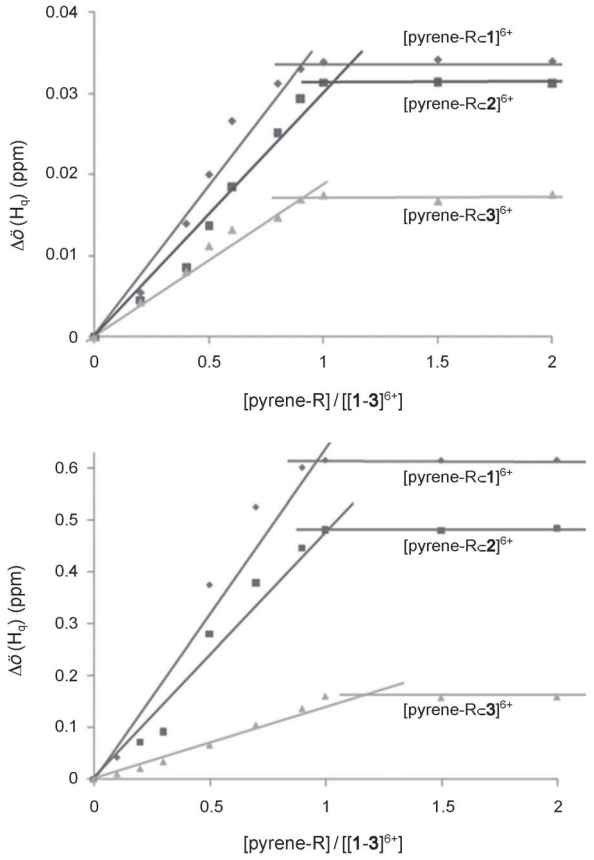

Figure 6. Changes in the ^{1}H NMR chemical shifts of the signal of the H_q protons of the *OO*∩*OO* ligands versus the molar ratio of pyrene-R/$[\mathbf{1}–\mathbf{3}]^{6+}$ in $(CD_3)_2SO$ at 21 °C (top) and of the signal of the H_β protons of the tpt ligands versus the molar ratio of pyrene-R/$[\mathbf{1}–\mathbf{3}]^{6+}$ in CD_3CN at 21 °C (bottom).

The determination of 1:1 stoichiometric systems allows us to represent the inclusion process of pyrene-R (guest) by the metalla-cages $[\mathbf{1}–\mathbf{3}]^{6+}$ (host) by Equation (1) in which k_+ and k_- define, respectively, the rate constants for association and dissociation of the [guest⊂host] system.

$$[\text{guest}] + [\text{host}] \underset{k_-}{\overset{k_+}{\rightleftharpoons}} [\text{guest} \subset \text{host}] \quad (1)$$

The quotient k_+/k_- of the rate constants for the formation and dissociation of the host–guest system gives the thermodynamic constant K and, at equilibrium, this stability constant can be defined by Equation (2).

$$K = \frac{k_+}{k_-} = \frac{[\text{guest} \subset \text{host}]}{[\text{guest}][\text{host}]} \quad (2)$$

Consequently, from the plots obtained for the ^{1}H NMR titrations, thermodynamic stability constants were estimated by using the non-linear least-squares fitting program winEQNMR2[26] (see Table 1). The values obtained show

Table 1. Stability constants (K) and Gibbs free energies ($\Delta G°$) for the encapsulation of pyrene-R in $[\mathbf{1}–\mathbf{3}]^{6+}$ determined by ^{1}H NMR titration.

[Guest⊂host] system	K [10^4 M^{-1}]	$\Delta G°$ [kcal mol^{-1}]
CD_3CN[a]		
[pyrene-R⊂**1**]$^{6+}$	4.1	−6.27
[pyrene-R⊂**2**]$^{6+}$	2.0	−5.86
[pyrene-R⊂**3**]$^{6+}$	1.2	−5.56
$(CD_3)_2SO$[b]		
[pyrene-R⊂**1**]$^{6+}$	4.4	−6.32
[pyrene-R⊂**2**]$^{6+}$	3.5	−6.19
[pyrene-R⊂**3**]$^{6+}$	2.4	−5.97

[a] Titration in CD_3CN at 21 °C with 4.0 mM concentration of the metalla-prisms. [b] Titration in $(CD_3)_2SO$ at 21 °C with 10.0 mM concentration of the metalla-prisms.

that at equilibrium (at constant temperature and for a given concentration and solvent), the equilibrium is strongly shifted towards the associative complexes [pyrene-R⊂**1**–**3**]$^{6+}$ rather than towards the dissociative species. The Gibbs free energies ($\Delta G°$) for the [pyrene-R⊂**1**–**3**]$^{6+}$ systems were then determined from the corresponding stability constants obtained at 21 °C in both CD_3CN and $(CD_3)_2SO$ from the Gibbs free-energy equation.[25]

In contrast to the carceplex system [pyrene-R⊂Ru_6(*p*-*i*PrC_6H_4Me)$_6$(tpt)$_2$(dobq)$_3$]$^{6+}$, in which the fluorescence of the pyrene-R guest was totally quenched upon encapsulation,[18] some fluorescence remains in the host–guest systems [pyrene-R⊂**1**–**3**]$^{6+}$ (see Figure 7). Indeed, the fluorescence of the pyrenyl part is quenched but the triazin-2-yl group does not entirely lose its fluorescent property. The quenching of the emission of the pyrenyl unit can be explained by

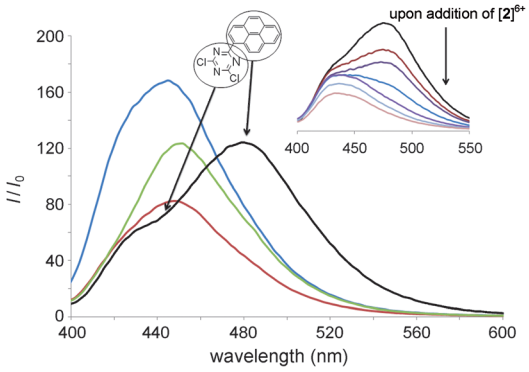

Figure 7. Fluorescence emission spectra of pyrene-R (black curve) and [pyrene-R⊂**1**–**3**]$^{6+}$ (blue curve = [pyrene-R⊂**1**]$^{6+}$, red curve = [pyrene-R⊂**2**]$^{6+}$, green curve = [pyrene-R⊂**3**]$^{6+}$) as solutions (10^{-7} M) in H_2O/DMSO (99.5:0.5, v/v) at 21 °C. Excitation at 350 nm. Inset: titration at 21 °C of [**2**][CF_3SO_3]$_6$ (0.1–6.0 equiv) versus a solution containing pyrene-R under the same conditions.

the summation of two electronic effects. First, as the pyrenyl part is trapped in the cavity of the metalla-prism, a fraction of the excitation energy normally absorbed by this guest molecule is intercepted by the host molecule, that is, static quenching. Secondly, quenching can also result from energy transfer from the pyrenyl group to the metalla-prism. Indeed, due to good spectral overlap of the absorbance of metalla-prisms $[\mathbf{1}–\mathbf{3}]^{6+}$ with the pyrenyl emission, energy transfer can spontaneously take place, thus leading to a decrease in the emission energy of the pyrenyl moiety and ultimately to fluorescence quenching.[27] On the other hand, because the triazin-2-yl group dangles out of the cavity of the metalla-prism, these two effects are not observed and thus the fluorescence intensity of this triazin-2-yl unit is conserved. This partial quenching of the fluorescence of pyrene-R in metalla-prisms $[\mathbf{1}–\mathbf{3}]^{6+}$ is illustrated by the emission spectra from the fluorescence titrations (see Figure 7). Upon gradual addition of $[\mathbf{1}–\mathbf{3}][CF_3SO_3]_6$ (0.1–6.0 equiv) to a H_2O/DMSO (99.5:0.5, v/v) solution of pyrene-R (10^{-7} M), the emission spectra (excitation: 350 nm, 21 °C) show a strong quenching of the band associated with the pyrenyl part, whereas the band associated with the triazin-2-yl group is less affected by the addition of $[\mathbf{1}–\mathbf{3}]^{6+}$.

Because we were unable to obtain an X-ray crystal structure of any of the host–guest systems, molecular modelling in the gas phase using the HyperChem software was used to construct each metalla-prism and the outputs of the simulations are presented in Figure 8.[28] These molecular dynamics simulations allow the portal sizes of these cages to be estimated in the gas phase. The largest portal, estimated to be approximately 7.4×10.2 Å^2, is found in [pyrene-R⊂**1**]$^{6+}$, which exhibits the highest fluorescence, that is, the most facile loss of the pyrene-R guest. Compound [pyrene-R⊂**3**]$^{6+}$, which contains the smallest portal (7.4×7.8 Å^2), exhibits the least fluorescence, which corresponds to a more stable host–guest system. These observations are in line with the free energies determined for these systems (see Table 1) and the release of the guest correlates very well with the corresponding portal sizes.

To assess the ability of the metalla-cages to improve the efficacy of biologically active compounds, the cytotoxicities of the cages, alone or with the pyrene-R or $Pd(acac)_2$ guests, were established on the A2780 ovarian cancer cell line (Table 2). The cytotoxicities of the two ′free′ guest molecules, pyrene-R and $Pd(acac)_2$, could not be determined due to their poor solubility. The cytotoxicities of pyrene-R and $Pd(acac)_2$ inside the cage systems is systematically higher than that of the corresponding cages. Moreover, the [Pd-$(acac)_2$⊂**1**–**3**]$^{6+}$ systems are more cytotoxic than the corresponding [pyrene-R⊂**1**–**3**]$^{6+}$ systems, behaviour that is consistent with other supramolecular drug systems.[18] The IC_{50} values indicate that the cage–guest complex acts as a drug-delivery system with the cage ensuring entry of the guest into the cancer cells, with the pyrene-R or $Pd(acac)_2$ acting on cell metabolism following intracellular release.

Table 2. Cytotoxicity of compounds towards A2780 cells (72 h incubation).

Compound	IC_{50} [μM]	SD [μM]
pyrene-R	ND	ND
$Pd(acac)_2$	ND	ND
[**1**][CF_3SO_3]$_6$	3.2	1.1
[**2**][CF_3SO_3]$_6$	13.1	1.1
[**3**][CF_3SO_3]$_6$	4.1	0.1
[pyrene-R⊂**1**][CF_3SO_3]$_6$	1.9	0.1
[pyrene-R⊂**2**][CF_3SO_3]$_6$	2.3	0.6
[pyrene-R⊂**3**][CF_3SO_3]$_6$	1.1	0.2
[$Pd(acac)_2$⊂**1**][CF_3SO_3]$_6$	<0.3	ND
[$Pd(acac)_2$⊂**2**][CF_3SO_3]$_6$	0.9	0.3
[$Pd(acac)_2$⊂**3**][CF_3SO_3]$_6$	<0.3	ND

Because the efficacy of a drug is related to its ability to cross the cell membrane, size and lipophilicity are crucial properties that profoundly influence drug molecules.[29,30] To gain further insight into the modes of uptake of these host–guest systems, we measured the intracellular ruthenium content, which reflects the uptake of the metalla-cage and the intrinsic fluorescence of the pyrene. The uptake of ruthenium into the cells was determined for the [pyrene-R⊂**1**–**3**]$^{6+}$ systems by inductively coupled plasma mass spectroscopy (ICP-MS), which reveals that all the compounds enter the cells to essentially the same extent (see Figure 9A) and indicates a similar uptake mechanism for the three supramolecular complexes. As previously reported, the fluorescence of pyrene-R is partially quenched inside the ruthenium cage[18] and consequently fluorescence can be used to evaluate the release of free pyrene-R inside the A2780 cells. Interestingly, flow cytometric analysis of cells incubated with [pyrene-R⊂**1**–**3**]$^{6+}$ (see Figure 9A) reveals that the ratio between cell fluorescence and the intracellular ruthenium concentration varies as a function of the metalla-cage used to entrap the pyrene-R fluorophore. Essentially, there is a clear correlation between the portal size of the host and the release of pyrene-R.

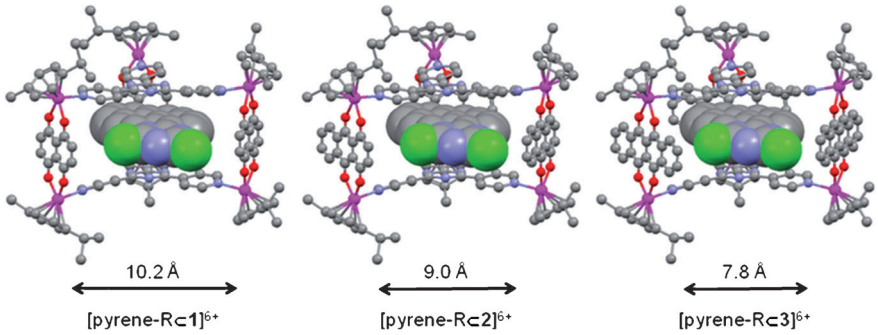

Figure 8. HyperChem simulations of the metalla-cages [pyrene-R⊂**1**–**3**]$^{6+}$.

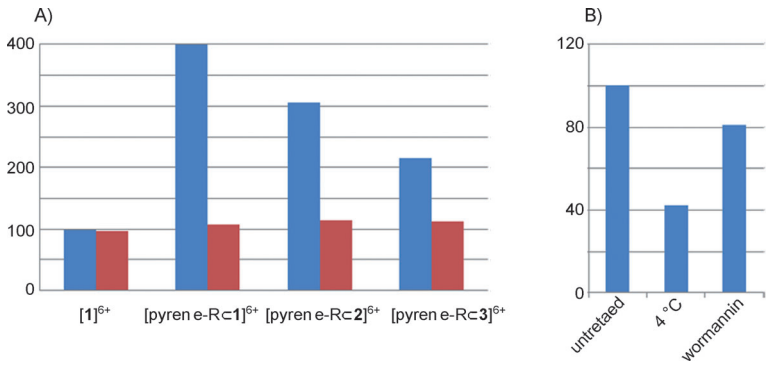

Figure 9. A) Fluorescence recorded by flow cytometry of [pyrene-R⊂**1**–**3**]$^{6+}$ indicating pyrene-R release from the host (blue). Ruthenium uptake determined by ICP-MS is also shown (red). Cells were incubated with [**1**]-[CF_3SO_3]$_6$ and [pyrene-R⊂**1**–**3**][CF_3SO_3]$_6$ at 2 μM for 24 h. B) Quantification of the intracellular fluorescence by flow cytometry of A2780 incubated with [pyrene-R⊂**1**]$^{6+}$ after 1 h pre-incubation in the culture medium (untreated; left), pre-incubated at 4 °C (centre) and pre-incubated with wortmannin (right). The results represent the percentage of fluorescence intensity relative to the untreated sample.

The mode of passage across the cell membrane of these molecules is also relevant. Due to their size, the molecules are putatively taken up by the cells by endocytosis, commonly assumed to be active, rather than by a cell-specific uptake mechanism on which an increasing amount of cancer research is focused.[29] The uptake mechanism of [pyrene-R⊂**1**]$^{6+}$ was also studied with uptake found to be both temperature- and wortmannin-sensitive (see Figure 9B). Wortmannin blocks specific endocytic mechanisms and has been widely used to study intracellular transport mechanisms.[30,31] Combined, these studies indicate that the uptake of [pyrene-R⊂**1**]$^{6+}$ involves endocytosis/macropinocytosis rather than passive diffusion across the cell membrane.

Following release of pyrene-R from the host, confocal microscopy was used to show that the pyrene-R stains vesicle-like cytoplasmic organelles and accumulates in the intracellular vesicle part of the cell endocytotic system.[32] A previous microscopy study showed that pyrene-R accumulates in cytoplasmic organelles.[18] In an attempt to better identify these organelles, their fluorescence pattern was compared with that of two known fluorescent reporters, the lysosomal dye Lysotracker Red and the fluid-phase endocytosis marker FITC-dextran (see Figure 10).[33] After 24 h of incubation, the free pyrene-R does not enter lysosomal compartments and does not accumulate in the endocytic compartments that are enriched in FITC-dextran, which suggests that pyrene-R accumulates in endocytic rather than lytic compartments. Hence, it would appear that the [**1**–**3**]$^{6+}$ drug carriers promote the accumulation of pyrene-R in a compartment in which protection from lysosomal and cytoplasmic detoxification takes place.

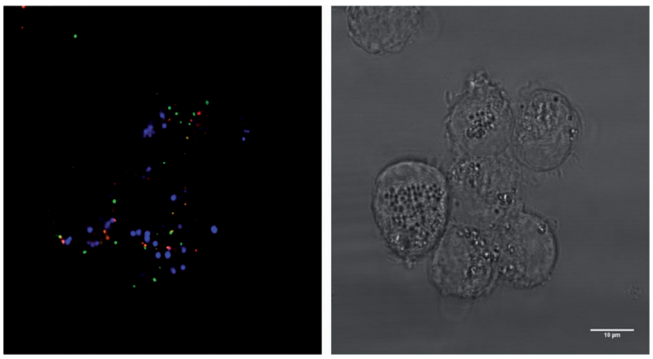

Figure 10. Confocal microscopy of A2780 cells incubated with [pyrene-R⊂**2**][CF_3SO_3]$_6$ at 2 μM for 24 h. Pyrene-R fluorescence (blue), FITC-dextran (green) and Lysotracker Red (red) were imaged. The fluorescence image is shown on the left and the transmitted-light picture on the right (scale bar = 10 μm).

Conclusion

We have described herein the synthesis, characterisation, host–guest properties and in vitro characterisation of a modular and adjustable supramolecular drug-delivery system based on hexaruthenium metalla-cages. Moreover, we have shown that the host molecules, which have similar sized cavities but different portal sizes, deliver their guests inside the cell with different efficiencies. Not only have cytotoxicity studies shown a synergistic effect between the metalla-cages and two non-related hydrophobic guest molecules, pyrene-R and Pd(acac)$_2$, but these studies also highlight other relevant features of this promising drug-delivery strategy. The portal size of the cage influences the ability to release the host. Nevertheless, all cages deliver the host to similar intracellular organelles. Through the use of specific inhibitors and fluorescent reporters, we have shown that endocytosis is probably involved in the uptake and leads to the accumulation of the guest molecule in intracellular organelles.

Experimental Section

2,4,6-Tris(pyridine-4-yl)-1,3,5-triazine (tpt)[34] and [Ru_2(*p*-*i*PrC_6H_4Me)$_2$-(*OO*∩*OO*)Cl_2] (*OO*∩*OO* = donq,[19] doaq[35] and dotq[24f]) were prepared according to published methods. 1-(4,6-Dichloro-1,3,5-triazin-2-yl)pyrene, Pd(acac)$_2$ and all other reagents were commercially available (Sigma–Aldrich) and used as received. All NMR measurements (^{1}H, ^{13}C{^{1}H}, 2D and DOSY) were recorded on a Bruker AMX 400 spectrometer using the residual protonated solvent as internal standard. Infrared spectra were recorded as KBr pellets on a Perkin–Elmer FTIR 1720-X spectrometer. UV/Vis absorption spectra were recorded on an Uvikon 930 spectrophotometer using precision cells made of quartz (1 cm). Fluorescence spectra were recorded on a Luminescence Perkin–Elmer LS50B spectrometer using precision cells made of quartz (1 cm). Elemental analyses were performed by the Mikroelementarisches Laboratorium, ETH

Zürich, or the Laboratory of Pharmaceutical Chemistry, University of Geneva (Switzerland).

For all DOSY experiments, the temperature was regulated at 298 K, the airflow was increased to 670 L min^{-1} and the NMR tube was spun. The diffusion NMR experiments were performed by using a standard pulsed-gradient stimulated echo (LED-PFGSTE) sequence using a bipolar gradient.[24] DOSY spectra were generated by using the TopSpin 2.0 software package.[36] Experimental parameters were $\Delta = 50.0$ ms (diffusion delay), $\tau = 1.0$ ms (gradient recovery delay) and $Te = 5.0$ ms (eddy current recovery delay). For each data set, 4096 complex points were collected and the gradient dimension was sampled in 16 experiments in which the gradient strength was gradually increased from 1.0 to 50.8 G cm^{-1}. The gradient duration $\delta/2$ was adjusted to observe a near complete signal loss at 50.8 G cm^{-1}. Typically, a $\delta/2$ delay of 1.2–2.0 ms was chosen. A 1.0 s recycle delay was used between scans for the data shown. For each data set, the spectral axis was processed with an exponential function (3–5 Hz line-broadening) and a Fourier transform was applied to obtain 4096 real points. The DOSY reconstruction was realised with 256 points in the diffusion dimension. The number of scans ranged from 8 to 64 and was adapted to each sample. The experimental time ranged from 4 to 30 min.

Syntheses of [guest⊂1–3][CF_3SO_3]$_6$: A mixture of $Ag(CF_3SO_3)$ (72 mg, 0.28 mmol), $[Ru_2(p\text{-cymene})_2(OO\cap OO)Cl_2]$ ($OO\cap OO$ = **1**: donq: 102 mg; **2**: doaq: 109 mg; **3**: dotq: 116 mg; 0.14 mmol), tpt (29 mg, 0.09 mmol) and guest molecule $Pd(acac)_2$ (14 mg, 0.05 mmol) or 1-(4,6-dichloro-1,3,5-triazin-2-yl)pyrene (17 mg, 0.05 mmol)in CH_3OH (30 mL) was stirred at 60 °C for 12 h. The solvent was then filtered and the residue was dissolved in CH_2Cl_2 (3 mL) and diethyl ether was slowly added to precipitate the solid, which was filtered and dried under vacuum.

[Pd(acac)$_2$⊂1][CF_3SO_3]$_6$: Yield: 143 mg (75 %); ^{1}H NMR (400 MHz, CD_3CN): $\delta = 8.60$ (d, ^3J(H,H) = 6.5 Hz, 12 H; H_α), 8.34 (d, ^3J(H,H) = 6.5 Hz, 12 H; H_β), 7.29 (s, 12 H; H_q), 5.70 (d, ^3J(H,H) = 5.9 Hz, 12 H; H_{cym}), 5.52 (d, 12 H; H_{cym}), 3.45 (m, 2 H; CH_{acac}), 2.80 (sept., ^3J(H,H) = 6.9 Hz, 6 H; CH(CH$_3$)$_2$), 2.10 (s, 18 H; CH_3), 1.30 (d, 36 H; CH(CH_3)$_2$), 0.02 ppm (m, 12 H; CH_{3acac}); ^{13}C{^{1}H} NMR (100 MHz, CD_3CN): $\delta = 172.0$ (CO), 170.1 (C_{tpt}), 156.2 (CH_α), 147.0 (C_{tpt}), 135.4 (CH_q), 123.9 (CH_β), 111.5 (C_q), 103.8 (C_{cym}), 102.0 (CH_{acac}), 100.5 (C_{cym}), 84.7 (CH_{cym}), 84.2 (CH_{cym}), 31.4 (CH(CH$_3$)$_2$), 23.1 (CH(CH_3)$_2$), 22.1 (CH(CH_3)$_2$), 17.4 (CH_3), 15.7 ppm (CH_{3acac}); IR (KBr): $\tilde{\nu} = 3060$ (w, CH_{aryl}), 1536 (s, C=O), 1260 cm^{-1} (s, CF_3); UV/Vis (1.0×10^{-5} M, CH_2Cl_2): λ_{max} (ε) = 308 (3.99×10^5), 374 (0.75×10^5), 526 (0.17×10^5), 568 (0.24×10^5), 612 nm (0.29×10^5 M^{-1} cm^{-1}); elemental analysis calcd (%) for $C_{142}H_{134}F_{18}N_{12}O_{34}PdRu_6S_6$: C 44.88, H 3.55, N 4.42; found: C 44.21, H 3.53, N 4.33.

[Pd(acac)$_2$⊂2][CF_3SO_3]$_6$: Yield: 147 mg (74 %); ^{1}H NMR (400 MHz, CD_3CN): $\delta = 8.81$ (m, 6 H; H_q), 8.64 (m, 12 H; H_α), 8.15 (m, 6 H; H_q), 8.05 (m, 12 H; H_β), 7.42 (m, 6 H; H_q), 5.81 (d, ^3J(H,H) = 5.6 Hz, 12 H; H_{cym}), 5.63 (d, 12 H; H_{cym}), 3.49 (m, 2 H; CH_{acac}), 2.81 (sept., ^3J(H,H) = 6.8 Hz, 6 H; CH(CH$_3$)$_2$), 2.11 (s, 18 H; CH_3), 1.30 (d, 36 H; CH(CH_3)$_2$), 0.02 ppm (m, 12 H; CH_{3acac}); ^{13}C{^{1}H} NMR (100 MHz, CD_3CN): $\delta = 171.5$ (CO), 170.5 (CO), 169.9 (C_{tpt}), 157.9 (CH_α), 144.8 (C_{tpt}), 139.8 (CH_q), 134.7 (CH_q), 129.6 (CH_q), 124.9 (CH_β), 110.7 (C_q), 103.8 (C_{cym}), 102.0 (CH_{acac}), 101.2 (C_{cym}), 89.7 (CH_{cym}), 88.6 (CH_{cym}), 85.2 (CH_{cym}), 84.7 (CH_{cym}), 31.4 (CH(CH$_3$)$_2$), 22.5 (CH(CH_3)$_2$), 22.1 (CH(CH_3)$_2$), 17.6 (CH_3), 15.5 ppm (CH_{3acac}); IR (KBr): $\tilde{\nu} = 3060$ (w, CH_{aryl}), 1536 (s, C=O), 1260 cm^{-1} (s, CF_3); UV/Vis (1.0×10^{-5} M, CH_2Cl_2): λ_{max} (ε) = 308 (3.95×10^5), 371 (0.66×10^5), 447 (0.50×10^5), 648 nm (0.22×10^5 M^{-1} cm^{-1}); elemental analysis calcd (%) for $C_{154}H_{140}F_{18}N_{12}O_{34}PdRu_6S_6$: C 46.83, H 3.57, N 4.26; found: C 46.31, H 3.54, N 4.15.

[Pd(acac)$_2$⊂3][CF_3SO_3]$_6$: Yield: 157 mg (77 %); ^{1}H NMR (400 MHz, CD_3CN): $\delta = 8.80$ (dd, ^3J(H,H) = 6.3 Hz, ^4J(H,H) = 3.1 Hz, 12 H; H_q), 8.51 (d, ^3J(H,H) = 6.5 Hz, 12 H; H_α), 8.02 (m, 24 H; $H_q + H_\beta$), 5.90 (d, ^3J(H,H) = 6.1 Hz, 12 H; H_{cym}), 5.60 (d, 12 H; H_{cym}), 3.51 (m, 2 H; CH_{acac}), 2.79 (sept., ^3J(H,H) = 6.4 Hz, 6 H; CH(CH$_3$)$_2$), 2.10 (s, 18 H; CH_3), 1.30 (d, 36 H; CH(CH_3)$_2$), 0.02 ppm (m, 12 H; CH_{3acac}); ^{13}C{^{1}H} NMR (100 MHz, CD_3CN): $\delta = 170.0$ (CO), 165.7 (C_{tpt}), 152.2 (CH_α), 141.3 (C_{tpt}), 133.1 (C_q), 132.6 (CH_q), 127.0 (CH_q), 123.2 (CH_β), 106.5 (C_q), 103.4 (C_{cym}), 102.2 (CH_{acac}), 101.1 (C_{cym}), 85.2 (CH_{cym}), 85.1 (CH_{cym}), 84.8 (CH_{cym}), 84.6 (CH_{cym}), 31.2 (CH(CH$_3$)$_2$), 22.1 (CH(CH_3)$_2$), 22.0 (CH(CH_3)$_2$), 17.9 (CH_3), 15.8 ppm (CH_{3acac}); IR (KBr): $\tilde{\nu} = 3060$ (w, CH_{aryl}), 1536 (s, C=O), 1260 cm^{-1} (s, CF_3); UV/Vis (1.0×10^{-5} M, CH_2Cl_2): λ_{max} (ε) = 308 (3.90×10^5), 380 (0.56×10^5), 607 (0.20×10^5), 655 nm (0.22×10^5 M^{-1} cm^{-1}); elemental analysis calcd (%) for $C_{166}H_{146}F_{18}N_{12}O_{34}PdRu_6S_6$: C 48.63, H 3.59, N 4.10; found: C 47.92, H 3.57, N 4.02.

[Pyrene-R⊂1][CF_3SO_3]$_6$: Yield: 149 mg (77 %); ^{1}H NMR (400 MHz, CD_3CN): $\delta = 8.40$ (d, ^3J(H,H) = 6.6 Hz, 12 H; H_α), 7.78 (m, 12 H; H_β), 7.47 (s, 12 H; H_q), 7.25 (m, 1 H; H_{pyr}), 7.08 (m, 1 H; H_{pyr}), 6.12 (m, 1 H; H_{pyr}), 5.82 (m, 1 H; H_{pyr}), 8.75 (m, 1 H; H_{pyr}), 5.69 (d, ^3J(H,H) = 5.7 Hz, 12 H; H_{cym}), 5.44 (d, 12 H; H_{cym}), 5.22 (m, 1 H; H_{pyr}), 4.92 (m, 1 H; H_{pyr}), 4.81 (m, 1 H; H_{pyr}), 4.75 (m, 1 H; H_{pyr}), 2.80 (sept., ^3J(H,H) = 6.7 Hz, 6 H; CH-(CH$_3$)$_2$), 2.07 (s, 18 H; CH_3), 1.32 ppm (d, 36 H; CH(CH_3)$_2$); ^{13}C{^{1}H} NMR (100 MHz, CD_3CN): $\delta = 171.2$ (CO), 170.5 (C_{tpt}), 155.1 (CH_α), 144.3 (C_{tpt}), 139.9 (CH_q), 130.8 (C_{pyr}), 128.6 (CH_{pyr}), 127.8 (CH_{pyr}), 126.6 (C_{pyr}), 126.2 (CH_β), 115.5 (C_q), 104.8 (C_{cym}), 100.4 (C_{cym}), 85.1 (CH_{cym}), 84.6 (CH_{cym}), 31.4 (CH(CH$_3$)$_2$), 23.0 (CH(CH_3)$_2$), 22.1 (CH(CH_3)$_2$), 17.3 ppm (CH_3); IR (KBr): $\tilde{\nu} = 3060$ (w, CH_{aryl}), 1536 (s, C=O), 1500 (m, C=C), 1260 cm^{-1} (s, CF_3); UV/Vis (1.0×10^{-5} M, CH_2Cl_2): λ_{max} (ε) = 308 (3.88×10^5), 377 (0.47×10^5), 563 (0.24×10^5), 613 nm (0.17×10^5 M^{-1} cm^{-1}); elemental analysis calcd (%) for $C_{151}H_{129}Cl_2F_{18}N_{15}O_{30}Ru_6S_6$: C 47.16, H 3.38, N 5.46; found: C 47.08, H 3.46, N 5.42.

[Pyrene-R⊂2][CF_3SO_3]$_6$: Yield: 146 mg (73 %); ^{1}H NMR (400 MHz, CD_3CN): $\delta = 8.78$ (m, 6 H; H_q), 8.60 (m, 12 H; H_α), 8.09 (m, 6 H; H_q), 8.01 (m, 12 H; H_β), 7.96 (m, 1 H; H_{pyr}), 7.71 (m, 1 H; H_{pyr}), 7.40 (m, 6 H; H_q), 7.21 (m, 1 H; H_{pyr}), 7.01 (m, 1 H; H_{pyr}), 5.98 (m, 1 H; H_{pyr}), 5.81 (d, ^3J-(H,H) = 5.8 Hz, 12 H; H_{cym}), 5.62 (d, 12 H; H_{cym}), 5.52 (m, 1 H; H_{pyr}), 5.09 (m, 1 H; H_{pyr}), 4.96 (m, 1 H; H_{pyr}), 4.75 (m, 1 H; H_{pyr}), 2.80 (sept., ^3J-(H,H) = 6.7 Hz, 6 H; CH(CH$_3$)$_2$), 2.10 (s, 18 H; CH_3), 1.29 ppm (d, 36 H; CH(CH_3)$_2$); ^{13}C{^{1}H} NMR (100 MHz, CD_3CN): $\delta = 170.5$ (CO), 170.2 (CO), 169.8 (C_{tpt}), 156.7 (CH_α), 142.4 (C_{tpt}), 141.0 (CH_q), 135.6 (CH_q), 130.2 (CH_q), 129.7 (C_{pyr}), 128.2 (CH_{pyr}), 126.8 (CH_{pyr}), 126.2 (C_{pyr}), 125.9 (CH_β), 109.1 (C_q), 104.9 (C_{cym}), 101.1 (C_{cym}), 88.6 (CH_{cym}), 87.8 (CH_{cym}), 86.1 (CH_{cym}), 85.9 (CH_{cym}), 32.2 (CH(CH$_3$)$_2$), 22.9 (CH(CH_3)$_2$), 22.7 (CH-(CH_3)$_2$), 17.0 ppm (CH_3); IR (KBr): $\tilde{\nu} = 3060$ (w, CH_{aryl}), 1536 (s, C=O), 1500 (m, C=C), 1260 cm^{-1} (s, CF_3); UV/Vis (1.0×10^{-5} M, CH_2Cl_2): λ_{max} (ε) = 308 (3.79×10^5), 442 (0.36×10^5), 659 nm (0.18×10^5 M^{-1} cm^{-1}); elemental analysis calcd (%) for $C_{163}H_{135}Cl_2F_{18}N_{15}O_{30}Ru_6S_6$: C 49.00, H 3.41, N 5.26; found: C 48.91, H 3.48, N 5.22.

[Pyrene-R⊂3][CF_3SO_3]$_6$: Yield: 155 mg (75 %); ^{1}H NMR (400 MHz, CD_3CN): $\delta = 8.90$ (m, 12 H; H_α), 8.84 (m, 12 H; H_β), 8.11 (m, 12 H; H_q), 7.90 (m, 1 H; H_{pyr}), 7.75 (m, 1 H; H_{pyr}), 7.22 (m, 12 H; H_q), 7.18 (m, 1 H; H_{pyr}), 7.09 (m, 1 H; H_{pyr}), 6.31 (m, 1 H; H_{pyr}), 5.88 (d, ^3J(H,H) = 6.2 Hz, 12 H; H_{cym}), 5.61 (d, 12 H; H_{cym}), 5.35 (m, 1 H; H_{pyr}), 5.18 (m, 1 H; H_{pyr}), 4.88 (m, 1 H; H_{pyr}), 4.71 (m, 1 H; H_{pyr}), 2.80 (sept., ^3J(H,H) = 6.6 Hz, 6 H; CH(CH$_3$)$_2$), 2.09 (s, 18 H; CH_3), 1.32 ppm (d, 36 H; CH(CH_3)$_2$); ^{13}C{^{1}H} NMR (100 MHz, CD_3CN): $\delta = 171.1$ (CO), 166.9 (C_{tpt}), 151.3 (CH_α), 140.2 (C_{tpt}), 133.1 (C_q), 132.8 (CH_q), 131.2 (C_{pyr}), 128.9 (CH_{pyr}), 128.2 (CH_{pyr}), 127.4 (C_{pyr}), 126.9 (CH_q), 124.3 (CH_β), 105.5 (C_q), 104.8 (C_{cym}), 100.9 (C_{cym}), 85.4 (CH_{cym}), 85.3 (CH_{cym}), 85.1 (CH_{cym}), 84.9 (CH_{cym}), 31.0 (CH(CH$_3$)$_2$), 22.2 (CH(CH_3)$_2$), 20.9 (CH(CH_3)$_2$), 18.1 ppm (CH_3); IR (KBr): $\tilde{\nu} = 3060$ (w, CH_{aryl}), 1536 (s, C=O), 1500 (m, C=C), 1260 cm^{-1} (s, CF_3); UV/Vis (1.0×10^{-5} M, CH_2Cl_2): λ_{max} (ε) = 308 (3.60×10^5), 390 (0.23×10^5), 607 (0.14×10^5), 658 nm (0.13×10^5 M^{-1} cm^{-1}); elemental analysis calcd (%) for $C_{175}H_{141}Cl_2F_{18}N_{15}O_{30}Ru_6S_6$: C 50.70, H 3.43, N 5.07; found: C 49.97, H 3.41, N 4.97.

Culture and inhibition of cell growth: Human A2780 ovarian carcinoma cells were obtained from the European Centre of Cell Cultures (ECACC, Salisbury, UK) and maintained in culture as described by the provider. The cells were routinely grown in RPMI 1640 medium containing 10 % foetal calf serum (FCS) and antibiotics at 37 °C and under 5 % CO_2. To evaluate growth inhibition, the cells were seeded in 96-well plates (25 000 cells per well) and grown for 24 h in complete medium. Compounds were added to the cell culture to the required concentration and incubated for 72 h. Solutions of the compounds were applied by diluting a freshly prepared stock solution of the corresponding compound in DMSO, with the final concentration of 0.05 % in the medium. The 3-(4,5-dimethylthiazol-2-yl)-2,5-diphenyltetrazolium bromide (MTT) test was performed in the last 2 h without changing the culture medium. Following drug exposure, MTT (from Sigma) was added to the cells at a

final concentration of 0.2 mg mL^{-1} and incubated for 2 h, then the culture medium was aspirated and the violet formazan precipitate dissolved in DMSO. The optical density was quantified at 540 nm by using a multiwell plate reader (iEMS Reader MF, Labsystems, USA), and the percentage of surviving cells was calculated from the ratio of absorbance of treated to untreated cells. The IC_{50} values for the inhibition of cell growth were determined by fitting the plot of the percentage of surviving cells against the drug concentration using a sigmoidal function (Origin v7.5).[37]

Microscopy experiments: Cells were grown for 24 h on chambered coverglass (Lab-Tek, NUNC) slides in complete medium at a density of 1×10^4 cells per well and later exposed to the appropriate compound at 37 °C in the dark. Cells were stained with Lysotracker Red DND-99 (Invitrogen, Molecular Probes) and 10 kDa FITC-dextran (Invitrogen, Molecular Probes) for 30 min at 37 °C. Excess complex was washed away with PBS, fixed with 4 % formaldehyde in PBS for 30 min in the dark and rinsed twice with PBS before observation. Cells were mounted in PBS before being observed by confocal microscopy using a Zeiss LSM 700 inverted microscope equipped with a 40X oil immersion objective. Filters used for the excitation and detection of pyrene-R were 405 and 492 nm, respectively, 488 and 559 nm for the detection of FITC-dextran, and 555 and 587 nm for the detection of Lysotracker Red DND-99. The intensities of the fluorescence signals were evaluated by using the Zen software.[38]

Flow cytometry: Cells were detached from the culture with EDTA (0.48 mM in PBS) and incubated at 1×10^6 cells/mL with [pyrene-R⊂**1**–**3**]-$[CF_3SO_3]_6$ salts (added from a concentrated DMSO stock) under the conditions described above and then placed on ice. The fluorescence of ~20 000 cells was measured by using a BD LSR II analyser, exciting with a 355 nm laser for pyrene-R. Emission was observed at 450 ± 40 nm. The fluorescence data were analysed by using the FlowJo 8 software.[39]

[1] a) W. M. Nau, *Nat. Chem.* **2010**, *2*, 248–250; b) K. K. Cotí, M. E. Belowich, M. Liong, M. W. Ambrogio, Y. A. Lau, H. A. Khatib, J. I. Zink, N. M. Khashab, J. F. Stoddart, *Nanoscale* **2009**, *1*, 16–39; c) G. Wenz, *Clin. Drug Invest.* **2000**, *19*, 21–25.

[2] a) M. Vallet-Regí, F. Balas, D. Arcos, *Angew. Chem.* **2007**, *119*, 7692–7703; *Angew. Chem. Int. Ed.* **2007**, *46*, 7548–7558; b) E. Gabano, M. Ravera, D. Osella, *Curr. Med. Chem.* **2009**, *16*, 4544–4580.

[3] a) P. J. Dyson, G. Sava, *Dalton Trans.* **2006**, 1929–1933; b) S. H. van Rijt, P. J. Sadler, *Drug Discovery Today* **2009**, *14*, 1089–1097; c) C. Sanchez-Cano, M. J. Hannon, *Dalton Trans.* **2009**, 10702–10711.

[4] a) T. Boulikas, M. Vougiouka, *Oncol. Rep.* **2003**, *10*, 1663–1682; b) K. S. Lovejoy, S. J. Lippard, *Dalton Trans.* **2009**, 10651–10659.

[5] N. W. Shi Kam, T. C. Jessop, P. A. Wender, H. Dai, *J. Am. Chem. Soc.* **2004**, *126*, 6850–6851.

[6] Z. Yang, X. Wang, H. Diao, J. Zhang, H. Li, H. Sun, Z. Guo, *Chem. Commun.* **2007**, 3453–3455.

[7] a) A. M. Krause-Heuer, N. J. Wheate, M. J. Tilby, D. G. Pearson, C. J. Ottley, J. R. Aldrich-Wright, *Inorg. Chem.* **2008**, *47*, 6880–6888; b) N. J. Wheate, A. I. Day, R. J. Blanch, A. P. Arnold, C. Cullinane, J. G. Collins, *Chem. Commun.* **2004**, 1424–1425; c) N. J. Wheate, D. P. Buck, A. I. Day, J. G. Collins, *Dalton Trans.* **2006**, 451–458; d) N. J. Wheate, R. I. Taleb, A. M. Krause-Heuer, R. L. Cook, S. Wang, V. J. Higgins, J. R. Aldrich-Wright, *Dalton Trans.* **2007**, 5055–5064.

[8] a) J. M. Rademaker-Lakhai, C. Terret, S. B. Howell, C. M. Baud, R. F. de Boer, D. Pluim, J. H. Beijnen, J. H. M. Schellens, J. P. Droz, *Clin. Cancer Res.* **2004**, *10*, 3386–3395; b) M. Campone, J. M. Rademaker-Lakhai, J. Bennouna, S. B. Howell, D. P. Nowotnik, J. H. Beijnen, J. H. M. Schellens, *Cancer Chemother. Pharmacol.* **2007**, *60*, 523–533; c) P. Govender, N. C. Antonels, J. Mattsson, A. K. Renfrew, P. J. Dyson, J. R. Moss, B. Therrien, G. S. Smith, *J. Organomet. Chem.* **2009**, *694*, 3470–3476.

[9] Y. Matsumura, H. Maeda, *Cancer Res.* **1986**, *46*, 6387–6392.

[10] a) M. Fujita, M. Tominaga, A. Hori, B. Therrien, *Acc. Chem. Res.* **2005**, *38*, 369–380; b) B. H. Northrop, Y.-R. Zheng, K.-W. Chi, P. J. Stang, *Acc. Chem. Res.* **2009**, *42*, 1554–1563.

[11] a) F. A. Cotton, C. Y. Liu, C. A. Murillo, X. Wang, *Inorg. Chem.* **2006**, *45*, 2619–2626; b) M. D. Ward, *Chem. Commun.* **2009**, 4487–4499; c) C. Desmarets, F. Poli, X. F. Le Goff, K. Müller, H. Amouri, *Dalton Trans.* **2009**, 10429–10432; d) M. D. Pluth, R. G. Bergman, K. N. Raymond, *Acc. Chem. Res.* **2009**, *42*, 1650–1659; e) S. J. Dalgarno, N. P. Power, J. L. Atwood, *Coord. Chem. Rev.* **2008**, *252*, 825–841; f) A. Granzhan, T. Riis-Johannessen, R. Scopelliti, K. Severin, *Angew. Chem.* **2010**, *122*, 5647–5650; *Angew. Chem. Int. Ed.* **2010**, *49*, 5515–5518; g) W. Meng, B. Breiner, K. Rissanen, J. D. Thoburn, J. K. Clegg, J. R. Nitschke, *Angew. Chem.* **2011**, *123*, 3541–3545; *Angew. Chem. Int. Ed.* **2011**, *50*, 3479–3483.

[12] a) J. I. van der Vlugt, T. S. Koblenz, J. Wassenaar, J. N. H. Reek in *Molecular Encapsulation* (Eds.: U. H. Brinker, J.- L. Mieusset), Wiley, New York, **2010**, pp. 145–174; b) J.- L. Mieusset, U. H. Brinker in *Molecular Encapsulation* (Eds.: U. H. Brinker, J.-L. Mieusset), Wiley, New York, **2010**, pp. 269–308; c) M. Yoshizawa, J. K. Klosterman, M. Fujita, *Angew. Chem.* **2009**, *121*, 3470–3490; *Angew. Chem. Int. Ed.* **2009**, *48*, 3418–3438; d) M. Wang, V. Vajpayee, S. Shanmugaraju, Y.-R. Zheng, Z. Zhao, H. Kim, P. S. Mukherjee, K.-W. Chi, P. J. Stang, *Inorg. Chem.* **2011**, *50*, 1506–1512.

[13] a) A. V. Davis, K. N. Raymond, *J. Am. Chem. Soc.* **2005**, *127*, 7912–7919; b) M. D. Pluth, K. N. Raymond, *Chem. Soc. Rev.* **2007**, *36*, 161–171.

[14] a) W. Han Ang, P. J. Dyson, *Eur. J. Inorg. Chem.* **2006**, 4003–4018; b) A. F. A. Peacock, P. J. Sadler, *Chem. Asian J.* **2009**, *4*, 1890–1899; c) A. Levina, A. Mitra, P. A. Lay, *Metallomics* **2009**, *1*, 458–470; d) G. Süss-Fink, *Dalton Trans.* **2010**, *39*, 1673–1688.

[15] a) T. B. Rauchfuss, K. Severin in *Organic Nanostructures* (Eds.: J. L. Atwood, J. W. Steed), Wiley-VCH, Weinheim, **2008**, pp. 179–203; b) B. Therrien, *Eur. J. Inorg. Chem.* **2009**, 2445–2453; c) Y.-F. Han, W.-G. Jia, W.-B. Yu, G.-X. Jin, *Chem. Soc. Rev.* **2009**, *38*, 3419–3434.

[16] a) J. Mattsson, P. Govindaswamy, J. Furrer, Y. Sei, K. Yamaguchi, G. Süss-Fink, B. Therrien, *Organometallics* **2008**, *27*, 4346–4356; b) P. Govindaswamy, J. Furrer, G. Süss-Fink, B. Therrien, *Z. Anorg. Allg. Chem.* **2008**, *634*, 1349–1352; c) J. Mattsson, O. Zava, A. K. Renfrew, Y. Sei, K. Yamaguchi, P. J. Dyson, B. Therrien, *Dalton Trans.* **2010**, *39*, 8248–8255; d) A. Pitto-Barry, N. P. E. Barry, O. Zava, R. Deschenaux, P. J. Dyson, B. Therrien, *Chem. Eur. J.* **2011**, *17*, 1966–1971.

[17] B. Therrien, G. Süss-Fink, P. Govindaswamy, A. K. Renfrew, P. J. Dyson, *Angew. Chem.* **2008**, *120*, 3833–3836; *Angew. Chem. Int. Ed.* **2008**, *47*, 3773–3776.

[18] O. Zava, J. Mattsson, B. Therrien, P. J. Dyson, *Chem. Eur. J.* **2010**, *16*, 1428–1431.

[19] N. P. E. Barry, B. Therrien, *Eur. J. Inorg. Chem.* **2009**, 4695–4700.

[20] J. Freudenreich, N. P. E. Barry, G. Süss-Fink, B. Therrien, *Eur. J. Inorg. Chem.* **2010**, 2400–2405.

[21] I. Mathew, Y. Li, Z. Li, W. Sun, *Dalton Trans.* **2010**, *39*, 11201–11209.

[22] D. Astruc, *Chimie Organométallique*, EDP Sciences, Les Ulis, **2000**, pp. 31–54.

[23] A. Pitto-Barry, N. P. E. Barry, O. Zava, R. Deschenaux, B. Therrien, *Chem. Asian J.* **2011**, *6*, 1595–1603.

[24] a) D. Wu, A. Chen, C. S. Johnson, Jr., *J. Magn. Reson. Ser. A.* **1995**, *115*, 123–126; b) C. S. Johnson, Jr., *Prog. Nucl. Magn. Reson. Spectrosc.* **1999**, *34*, 203–256; c) D. Ajami, J. Rebek, Jr., *Angew. Chem.* **2007**, *119*, 9443–9446; *Angew. Chem. Int. Ed.* **2007**, *46*, 9283–9286; d) J.-F. Lemonnier, S. Floquet, A. Kachmar, M.- M. Rohmer, M. Bénard, J. Marrot, E. Terazzi, C. Piguet, E. Cadot, *Dalton Trans.* **2007**, 3043–3054; e) N. P. E. Barry, J. Furrer, J. Freudenreich, G. Süss-Fink, B. Therrien, *Eur. J. Inorg. Chem.* **2010**, 725–728; f) N. P. E. Barry, J. Furrer, B. Therrien, *Helv. Chim. Acta* **2010**, *93*, 1313–1328.

[25] Y. Tsukube, H. Furuta, A. Odani, Y. Takeda, Y. Kudo, Y. Inoue, Y. Liu, H. Sakamoto, K. Kimura in *Comprehensive Supramolecular Chemistry* (Eds.: J. L. Atwood, J. E. D. Davies, D. D. Macnicol, F. Vögtle), Pergamon Press, Oxford, **1996**, pp. 425–482.

[26] M. J. Hynes, *J. Chem. Soc. Dalton Trans.* **1993**, 311–312.

[27] N. Bouquin, V. L. Malinovskii, R. Häner, *Chem. Commun.* **2008**, 1974–1976.
[28] HyperChem Computational Chemistry Software Package Version 7.5, Hypercube Inc., Gainesville, Florida (**2003**).
[29] A. C. Eifler, C. S. Thaxton, *Methods Mol. Biol.* **2011**, *726*, 325–338.
[30] R. Kjeken, S. A. Mousavi, A. Brech, G. Griffiths, T. Berg, *Biochem. J.* **2001**, *357*, 497–503.
[31] S. Falcone, E. Cocucci, P. Podini, T. Kirchhausen, E. Clementi, J. Meldolesi, *J. Cell Sci.* **2006**, *119*, 4758–4769.
[32] C. A. Puckett, J. K. Barton, *J. Am. Chem. Soc.* **2009**, *131*, 8738–8739.
[33] W. I. Lencer, P. Weyer, A. S. Verkman, D. A. Ausiello, D. Brown, *Am. J. Physiol.* **1990**, *258*, C309–C317.
[34] H. L. Anderson, S. Anderson, J. K. M. Sanders, *J. Chem. Soc. Perkin Trans. 1* **1995**, 2231–2245.
[35] F. Kühlwein, K. Polborn, W. Beck, *Z. Anorg. Allg. Chem.* **1997**, *623*, 1931–1944.
[36] TopSpin Software, Version 2.0, Bruker BioSpin, Rheinstetten, **2005**.
[37] Origin Scientific Graphing and Data Analysis Software, Version 7.5, OriginLab, Northampton, **2006**.
[38] Zen Software, Carl Zeiss MicroImaging, Germany, **2007**.
[39] FlowJo Software, Version 8.0 for the Analysis of Flow Cytometry Data, Tree Star, Stanford, **2006**.